Biosensors and Bioelectronics 167 (2020) 112486

Contents lists available at ScienceDirect

Biosensors and Bioelectronics

journal homepage: http://www.elsevier.com/locate/bios

Electrochemical detection of methyl parathion via a novel biosensor tailored on highly biocompatible electrochemically reduced graphene oxide-chitosan-hemoglobin coatings

Ranjeet Kaur [a], Shweta Rana [a,*], Kanika Lalit [a], Parkash Singh [b], Khushwinder Kaur [a]

[a] Department of Chemistry, Panjab University, Chandigarh, 160014, India
[b] Department of Mechanical Engineering, Malout Institute of Management and Informational Technology, Malout, 152107, India

ARTICLE INFO

Keywords:
Biocompatible
Hemoglobin immobilization
Electrochemical impedance spectroscopy (EIS)
Randles-equivalent circuit
Square wave voltammetry (SWV)
Methyl parathion
Real time monitoring

ABSTRACT:

A quick electrochemical sensing tool by utilizing novel bioelectrode based on redox active protein hemoglobin (Hb) has been offered here for the determination of methylparathion (MP). The bioelectrode has been designed by immobilizing Hb on electrochemically reduced graphene oxide-chitosan (ERGO-CS/Hb/FTO) based biocompatible coatings. Fourier transform-infrared analyses (FTIR), field emission scanning electron microscopy (FESEM), UV–visible and electrochemical characterization reveal the successful grafting of ERGO-CS/Hb/FTO. A detailed impedimetric analysis shows low charge transfer resistance (R_{CT}) and solution resistance (Rs) for the fabricated biosensor, thus pointing towards improved electrochemical performance and sensitivity. In-depth elucidation of redox analysis has been presented in terms of surface concentration of redox moiety (2.92×10^{-9} mol cm^{-2}) and heterogeneous electron transfer rate constant (0.0032 s^{-1}) which indicate enhanced surface coverage and better charge transfer properties of the proposed electrochemical biosensor. The sensor is equipped with a low limit of detection of 79.77 nM and a high sensitivity of 45.77 Acm^{-2} μM^{-1} with excellent reproducibility. The modified biosensor also offered its credibility towards detection of MP in vegetable samples with recovery (%) ranging from 94% to 101%. The designed biosensor hereby, evolves as a promising approach for the recognition of MP.

1. Introduction

Organophosphorus pesticides (OPs) are the most commonly used pest control management approach in the field of agriculture owing to their low-cost, high activity, ease of access and simplicity of manufacturing (Derbalah et al., 2019). Among the diverse range of OPs and their derivatives, methylparathion (MP) is one of the conventional nitro-aromatic compounds widely used in hatcheries, agricultural practices and fisheries due to the inexpensiveness and exorbitant insecticidal properties. However, the ability to interfere with neurological functions, health and reproductive defects makes it "extremely hazardous" as classified by WHO(Kovida et al., 2020; WHO, 2009). The serious health threats associated with MP leads to lethal carcinogenic poisoning causing abdominal pain, respiratory problems, eye pain, paralysis and even death (Thota and Ganesh, 2016; Tian et al., 2018), ultimately making them a target for their determination (Sahub et al., 2018). The conventional methods like chromatography (Balsebre et al., 2018), ELISA (Xu et al., 2012) and spectrophotometric methods (Qiao et al., 2018) for the determination of MP are limited to long analysis time, complex measurement procedure, extensive labor and hence irrational for field analysis. The advent of bioanalytical approach (portable, high selectivity and offer commercial applications) that can compete with existing technologies is enthralling researchers in this field. Amongst the recently developed biosensors, the most commonly ones are the electrochemical biosensors, as they offer miniaturization and portability, improved sensitivity and enhanced limit of detection (Facure et al., 2017). In this regard, electrochemical biosensors based on acetylcholinesterase (AChE) as the bio-recognition element have been used extensively for the detection of MP (Rana et al., 2019; Arjmand et al., 2017). But, these AChE based biosensors require the use of substrate to generate the electrochemical response (Rana et al., 2019). Henceforth, the need of a biosensor based on other enzymes, for sensing of MP is always an alternative choice to acquire selectivity, cost-effective and substrate free approach.

* Corresponding author.
E-mail addresses: shweta0402@gmail.com, shweta0402@pu.ac.in (S. Rana).

https://doi.org/10.1016/j.bios.2020.112486
Received 25 May 2020; Received in revised form 25 July 2020; Accepted 28 July 2020
Available online 7 August 2020

In literature (Wen et al., 2016), electrochemical nature of hemoglobin (Hb) has been utilized for the effective determination of nitromethane owing to its low cost, easy availability, and electrocatalytic performance. However, direct electron transfer between Hb and electrode is a laborious process because of complex structure and instability at electrode surface. Considering this, a better immobilization method is always in demand to prevent electrode passivation and structure retainment. In this regard, film entrapment within biocompatible matrices is an interesting approach, providing a suitable microenvironment for proteins (Ahmad et al., 2018). Chitosan (CS), is one such interesting non-hazardous biopolymer, known for unique properties of biological renewability, hydrophilicity, biodegradability with good film forming ability and large mechanical strength (Wang et al., 2017). This has provoked us also to use CS as an electrode material but, relatively poor conductivity of CS inhibits its use (Baranwal et al., 2018). To address this, CS is often blended with nanomaterials such as titanium oxides, carbon nanotubes, reduced graphene oxide etc. that augment the electrical conductivity (Patel et al., 2019). Amongst these, particularly graphene based electrode materials have shown tremendous potential for the analysis of nitroaromatic organophosphorus compounds. This owes to their peculiar properties such as high surface area, large electron transfer rate (Rodriguez et al., 2018) together with lower background currents, wide potential window (Lavanya et al., 2018) and economic suitability for sensing. Moreover, the large delocalized π-electron system of RGO forms strong π-π stacking interaction with MP along with electrostatic and H-bonding facilitating the strong binding of latter on its surface to bring excellent electrocatalytic activity (Govindasamy et al., 2017). RGO can also combine with CS, through amide linkages and hence assist in synthesis of well dispersed and stable composite.

Considering this, here in the present work, well known AChE is replaced by Hb, a redox active moiety with better sensitivity and selectivity. For the immobilization of Hb, one step green synthesis of electrochemically reduced graphene oxide-chitosan layers (ERGO-CS) involving no toxic reductant, has been approached. The biocompatible ERGO-CS matrix facilitates the direct electron transfer from protein to underlying electrode without the loss of native protein structure. To the best of our knowledge, the proposed method is an entirely novel platform in the biosensing of OPs which has not been explored before and is accompanied with superior sensing attributes over other conventional biosensors.

2. Experimental

2.1. Reagents and instruments

Graphite powder, CS, MP, Fluorine -tin oxide glass substrates (FTOs) (surface resistivity 13Ω/Sq) and Hb (lyophilized powder) were used as obtained from Sigma-Aldrich. Potassium ferricyanide (K_3 [$Fe(CN)_6$]), potassium ferrocyanide (K_4 [$Fe(CN)_6$]), potassium permanganate ($KMnO_4$) and sodium nitrate ($NaNO_3$) were obtained from Qualigens. The deionized water was procured from mili-Q-system. Sodium hydrogen phosphate anhydrous, sodium phosphate monobasic dihydrate and all interferents (picric acid, aminophenol, trinitrotoluene, resorcinol and phenol) were obtained from Avra synthesis. FTOs used for working electrodes were thoroughly cleaned in basic soap solution, acidic solution of 30% HCl followed by double-distilled water and then with acetone prior to use.

UV–Visible (UV–Vis) absorption spectra were obtained in the spectral region of 4000–500 cm^{-1} on UV–visible spectrophotometer (JASCO V 530). Fourier transform infrared (FTIR) analysis for electrode characterization was done on Nicolet IS50 FTIR spectrophotometer in the range 500–4000 cm^{-1}. The surface morphological features of modified electrodes were studied using Field emission scanning electron microscopy (FESEM-HITACHISU8010) and BROOKER-XFLASH along with energy dispersive X-ray spectroscopic analysis (EDS). Atomic force microscopic (AFM) analysis was carried out using BRUKER-INNOVA microscope with antimony doped silicon tip in non-contact mode. The entire electrochemical studies were done using three electrode cell containing Ag/AgCl/KCl as a reference hooked with electrochemical software (Autolab/PGSTAT204N) with multichannel assembly. The square wave voltammetry (SWV) was done in phosphate buffer solution (PBS, pH 7) between the potential range of −1.2 V to +0.2 V at an amplitude of +0.25 V and frequency of 25 Hz. The three electrode setup contains modified FTOs as working electrode, with platinum as counter and Ag/AgCl as reference. For electrochemical determination of MP, certain parameters like amount of Hb, pH of electrolytic media, deposition potential and deposition time were optimized (For experimental details see ESM). Also, the optimization has been well analyzed using Taguchi analysis (ESM).

2.2. Fabrication of electrochemically reduced graphene oxide-chitosan based electrodes (ERGO-CS/FTO)

The synthesis of graphene oxide (GO) was carried out using modified Hummer's method (Hummers et al., 1958; Mani et al., 2017) (See ESM for detailed procedure). For the electrodeposition of ERGO-CS/FTO a dispersion of 50 mg of CS in 1% acetic acid solution was made with continuous stirring. The solution was sonicated for about 1–2 h, to which 25 mg of GO was added and stirred for 30 min. The solution was again sonicated and GO-CS dispersion thus obtained was used as electrodeposition bath. The electrode was fabricated via chronoamperometry at a constant potential for −1.5 V for 100 s and designated as ERGO-CS/FTO.

2.3. Fabrication of electrochemically reduced graphene oxide-chitosan/hemoglobin based biosensor (ERGO-CS/Hb/FTO)

The surface of ERGO-CS/FTO electrode was then modified with Hb as electroactive material, by simple method of immobilization using drop casting (10 μl) (Fig. 1). Hb (5 mg ml^{-1}) solution required for this purpose was prepared using PBS (pH 7). The modified electrode was then washed with PBS to remove the unbound Hb to obtain ERGO-CS/Hb/FTO.

3. Results and discussions

3.1. Current transients and nucleation-growth mechanism of ERGO-CS/FTO

To understand the nucleation growth mechanism occurring during electrodeposition,chronoamperometric studies were done while electrodepositing ERGO-CS/FTO at a fixed potential of −1.5 V for 100 s. A sudden decrease in current was observed due to the formation of double layer at the interphase of FTO and polymer composite containing electrolytic solution (Fig. S1). The rapid fall at the start of process is due to decrease in concentration of polymer composite in the vicinity of electrode surface caused by electroreduction forming dense and uniform layers as also depicted in the microstructural analysis later in this section (Zhang et al., 2016). Basic redox chemistry occurring at the surface of electrodes during film deposition comprises of the following two steps:

3.1.1. Solubilization of CS to obtain GO-CS composite

In the acidic aqueous solution, firstly CS gets solubilized by abstracting a proton from acidic medium (1% acetic acid solution). With increase in pH of the solution, reversible solubility process results into precipitation, which forms the basis of film fabrication in case of CS carrying composites (Fig. S2). To address the concern of poor interfacial interactions between intrinsic graphene and CS, causing failures in obtaining their composites, we have introduced GO (25 mg) into the above prepared CS solution. The functional groups present in GO has resulted in the enhancement of interfacial interactions (Jana et al., 2014).

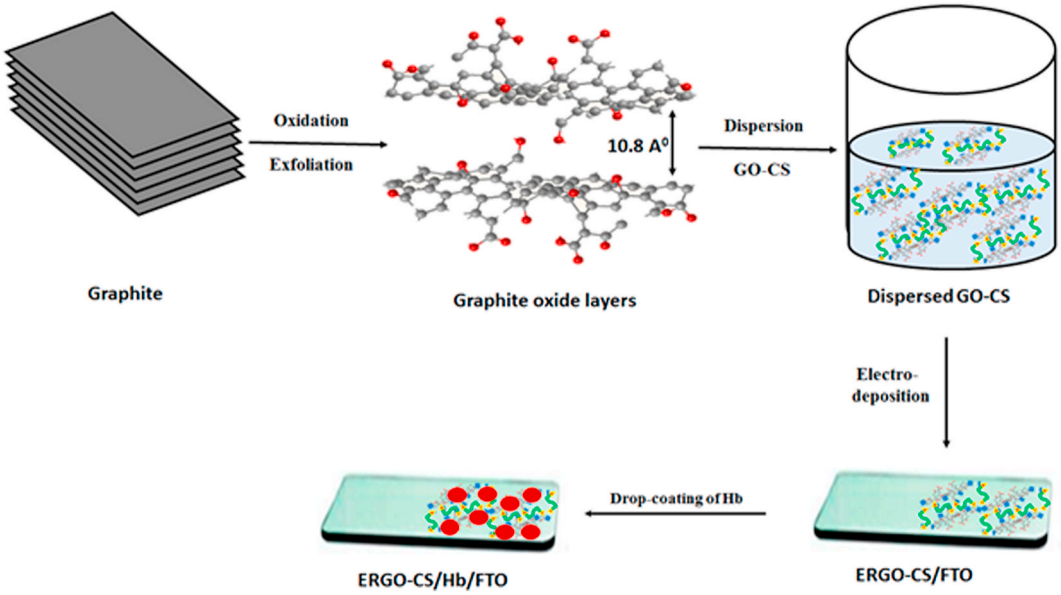

Fig. 1. Schematic diagram showing the fabrication of biosensor.

3.1.2. Reactions occurring at surface of FTO during electrodeposition of ERGO-CS/FTO

In case of chronoamperometry, a region of high pH is created near working electrode when held at sufficient negative potential, due to the reduction of H^+ ions (Eq. 1), which in turn deprotonates the GO-CS composites (Eq. 2) and hence gets deposited onto the electrode surface (Zangmeister et al., 2006). During electrodeposition, the electrode is held at sufficient negative potential that has resulted into the conversion of GO-CS to ERGO-CS as also depicted in FTIR analysis (Toh et al., 2014).

$$H^+ + e^- \rightarrow H_2 \quad (1)$$

$$GO\text{-}CS\text{-}NH_3^+ \rightarrow ERGO\text{-}CS\text{-}NH_2 \text{ (precipitation)} \quad (2)$$

3.2. UV–vis studies

In order to study the possible changes owing to the presence of heme, UV–Vis spectra of ERGO-CS & ERGO-CS/Hb have been taken (Fig. S3). It has been observed that for the Hb entrapped between the layers of ERGO-CS, the peak position of Soret band is at 404 nm while no absorption peak was perceptible in case of ERGO-CS/FTO. This suggests the successful entrapment of Hb between the layers of ERGO-CS (Jia et al., 2013). The position of Soret band at 404 nm is close to native Hb which advocates that native structure of Hb is retained even after immobilization on the electrode surface.

3.3. FTIR-studies

Fig. S4. shows the FTIR spectra of GO, ERGO/FTO, ERGO-CS/FTO and ERGO-CS/Hb/FTO for verifying the successful fabrication of electrodes. The FTIR spectra of GO shows a broad band between 3500 and 2500 cm^{-1} due to stretching of O–H group of carboxylic acid and alcohol functionalities along with absorbed water molecules on its surface. The band in the region of 1100–1400 cm^{-1} is due to C–O stretching of phenolic group whereas sharp peaks at 1031 $cm^{-1}$and 1700 cm^{-1}correspond to stretching vibrations of epoxy group and carbonyl group (C═O) of carboxylic acid respectively (Aliyev et al., 2019). The band at 1610 cm^{-1} is attributed to O–H bending of water molecules adsorbed on the surface of GO (Rana et al., 2019). This clearly infers the successful grafting of epoxy and carboxylic groups in basal and edge plane respectively, that further helps in immobilization of large amount of Hb onto the surface of prepared electrode (Navaee and Salimi, 2015; Shanmugharaj et al., 2013).

Upon one step reduction of GO, the magnitude of relative intensities of various oxygen functionalities decreases indicating the removal of most of the oxygen functionalities. Retaining of peak at 1610 cm^{-1} owing to C═C stretching and disappearance of C–H peak in FTIR spectra of RGO indicates the revival of sp^2 hybridized structure of graphene. Absence of peak at 1031 cm^{-1} again hints that epoxy groups are completely removed from the system(Jeyapragasam et al. (2013); (Toh et al., 2014). In case of RGO-CS/FTO the peak in the upper region (3500-2500 cm^{-1}) gets intensified due to interactions between carboxylic groups of GO and amine group of CS. The absorption bands of CS also appears at 1610-1690 cm^{-1} and 1500-1600 cm^{-1} corresponding to amide group I and II (Prabhakar et al., 2016).

The FTIR spectrum of ERGO-CS/Hb/FTO film exhibits the band at 1645 cm^{-1} and 1534 cm^{-1} corresponding to amide I and II of immobilized Hb (Zhang et al., 2014). This indicates that the innate structure of Hb has not been destroyed (Shan et al., 2007). This clearly points that ERGO-CS matrix is here providing a desirable microenvironment for the immobilization of Hb using the film entrapment.

3.4. Surface morphological studies

The surface morphological sketches of ERGO-CS/FTO and ERGO-CS/Hb/FTO electrodes were portrayed using FESEM. Fig. 2(a and b) corresponds to the FESEM images of ERGO-CS/FTO at lower and higher magnification respectively depicting sheet like morphology provided by RGO. The CS has been uniformly dispersed into the layers of RGO indicating entrapping of CS within layers of ERGO. In FESEM images of ERGO-CS/Hb/FTO (Fig. 2(c and d)), uniformly distributed spherical molecules of Hb are perceptible at both lower and higher magnification on the surface of ERGO-CS/FTO showing the successful immobilization of Hb enabled by excellent film forming ability of CS. Different oxygenous groups and edge defects in crumpled sheet like structures have enabled the loading of large amount of Hb. The EDS spectra of ERGO-CS/FTO and ERGO-CS/Hb/FTO films (inset of Fig. 2(b,d)) highlights the presence of different elements. The presence of Fe and N in ERGO-CS/Hb/FTO clearly shows the immobilization of Hb which is further authenticated by the elemental mapping of the films (Fig. 2(e)) as well as in AFM analysis (Fig. S5).

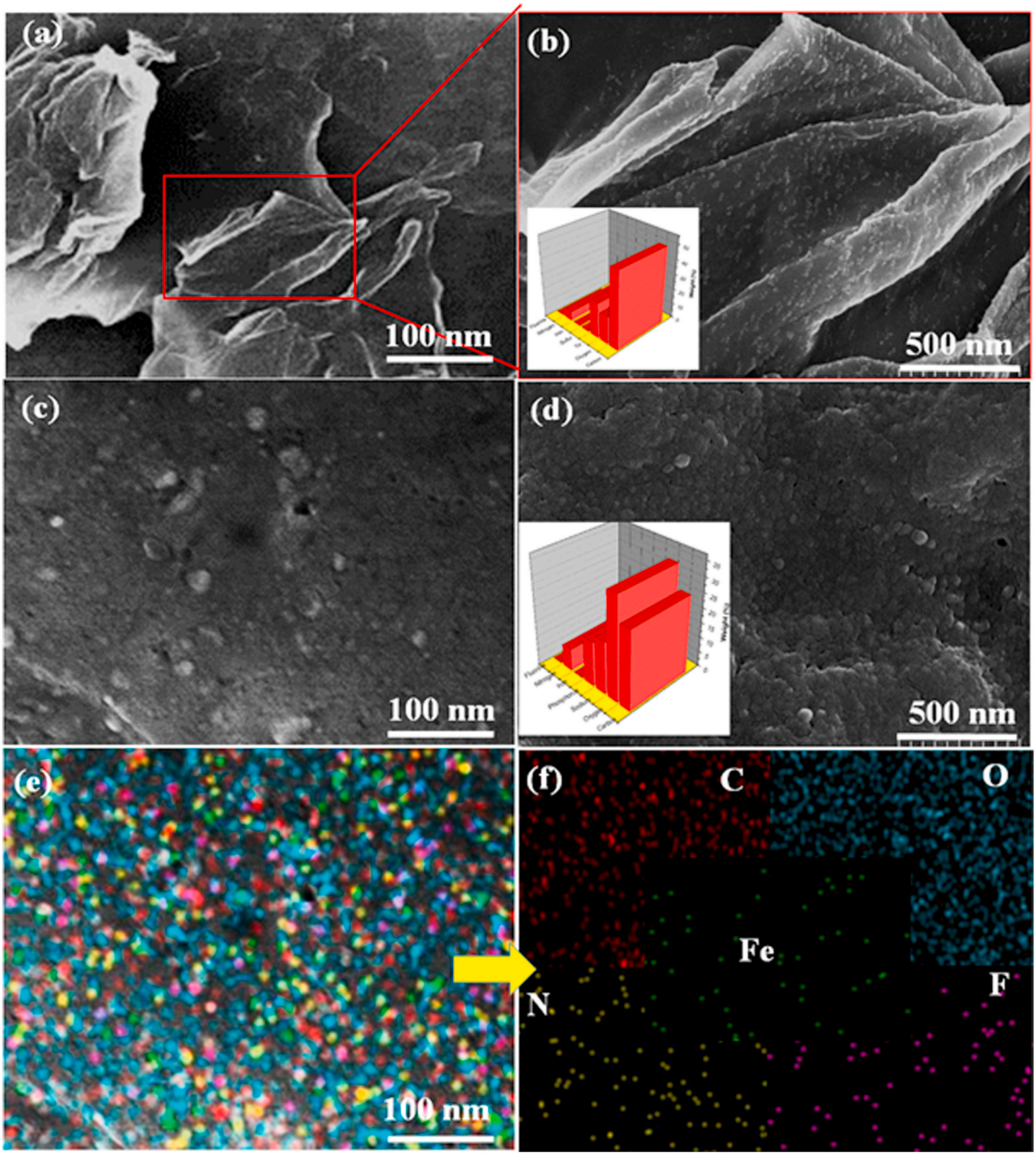

Fig. 2. FESEM images of (a) ERGO-CS/FTO at lower magnification and (b) at higher magnification (inset: EDS analysis) (c) ERGO-CS/Hb/FTO at lower magnification and (d) at higher magnification (inset: EDS analysis),(e) and (f) Elemental mapping of ERGO-CS/Hb/FTO.

3.5. Electrochemical studies of electrodes

The electrochemical attributes of all the prepared electrodes were analyzed using cyclic voltammetry (CV) between the potential range of −0.85 V to +1.0 V using $[Fe(CN)_6]^{3-/4-}$as redox couple (0.1 M KCl as redox probe in 0.1 M PBS (pH 7)). The ERGO-CS/Hb/FTO electrode consists of one anodic (A_2) and one cathodic peak (B_2) owing to appreciably fast charge transfer rate provided by the redox active centers of the heme group embedded between the layers of ERGO-CS/FTO. In contrast, peak strengths of ERGO-CS/FTO (A_1 and B_1) are very poor revealing rather apathetic charge transfer rate (Fig. 3). It is obvious from the voltammetric response that after the formation of protein layers on the surface of electrode the peak separation has contracted pointing towards the faster electron transfer kinetics (Lima et al., 2019).

The influence of scan rate onto ERGO-CS/Hb/FTO has also been investigated (Fig. S6). Using Eq. S1 (Thomas et al., 2015), the surface concentration of Hb comes out to be 2.92×10^{-9} mol cm^{-2} which is much larger than that of theoretically calculated monolayer coverage (1.89×10^{-11} mol cm^{-2}) (Zhang et al., 2014). Here, good biocompatibility and larger surface area provided by ERGO-CS/FTO, help to attain better surface coverage. The scan rate studies were also used to calculate heterogeneous electron transfer rate constant and thus the number of electrons 'n' being transferred in the reaction using Eq. S2 (Fotouhi et al., 2012). The value of 'n' came out to be 0.8 indicating the process to be one electron transfer, and the value of heterogeneous rate constant is 0.0032 s^{-1} which is better than already reported modified electrodes

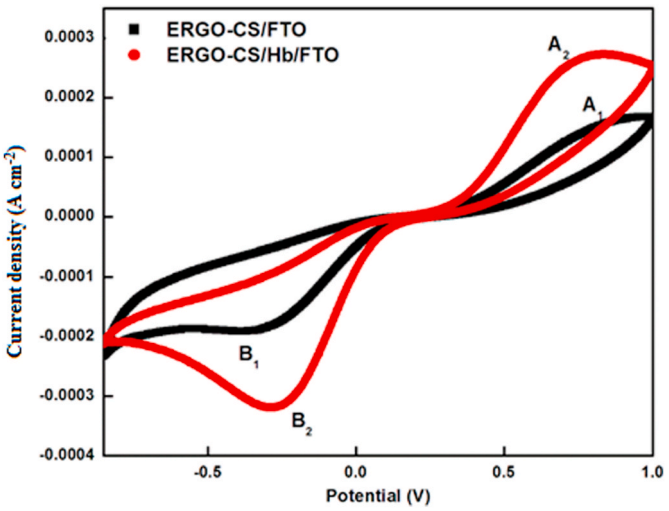

Fig. 3. CVs of ERGO-CS/FTO and ERGO-CS/Hb/FTO electrodes in PBS (pH 7) at scan rate 25 mV s^{-1} using $[Fe(CN)_6]^{3-/4-}$ in KCl as redox probe.

(Thomas et al., 2015), hinting at better charge transfer properties in this case.

3.6. Electrochemical impedance studies (EIS)

For further understanding the details of redox behavior, EIS representations were proposed within the frequency range of 0.01–10^5 Hz using $[Fe(CN)_6]^{3-/4-}$ in KCl as redox probe. Fig. 4 depicts the various EIS plots for ERGO-CS/FTO and ERGO-CS/Hb/FTO electrodes. A semicircle obtained in the middle frequency region in case of both the electrodes (Fig. 4(a)) is depictive of kinetically controlled phenomenon whereas a straight line perceptible in lower frequency region is indicative of the Warburg diffusion phenomenon. The diameter of semicircle indicative of R_{CT} gets reduced in ERGO-CS/Hb/FTO pointing towards its better electrochemical performance after immobilization of Hb.

To find the correlation of experimental data with the theoretical one, the Nyquist plots are best modelled using randles-equivalent circuits. The solid electrode based on ERGO-CS/FTO showed more reliable R_{CT} values with conventional Rs [Q (R_{ct}W)] as an equivalent circuit. However, after immobilization of Hb in ERGO-CS/Hb/FTO the interfacial properties were better described by R_S [C (R_{CT}W)] with lesser fitting

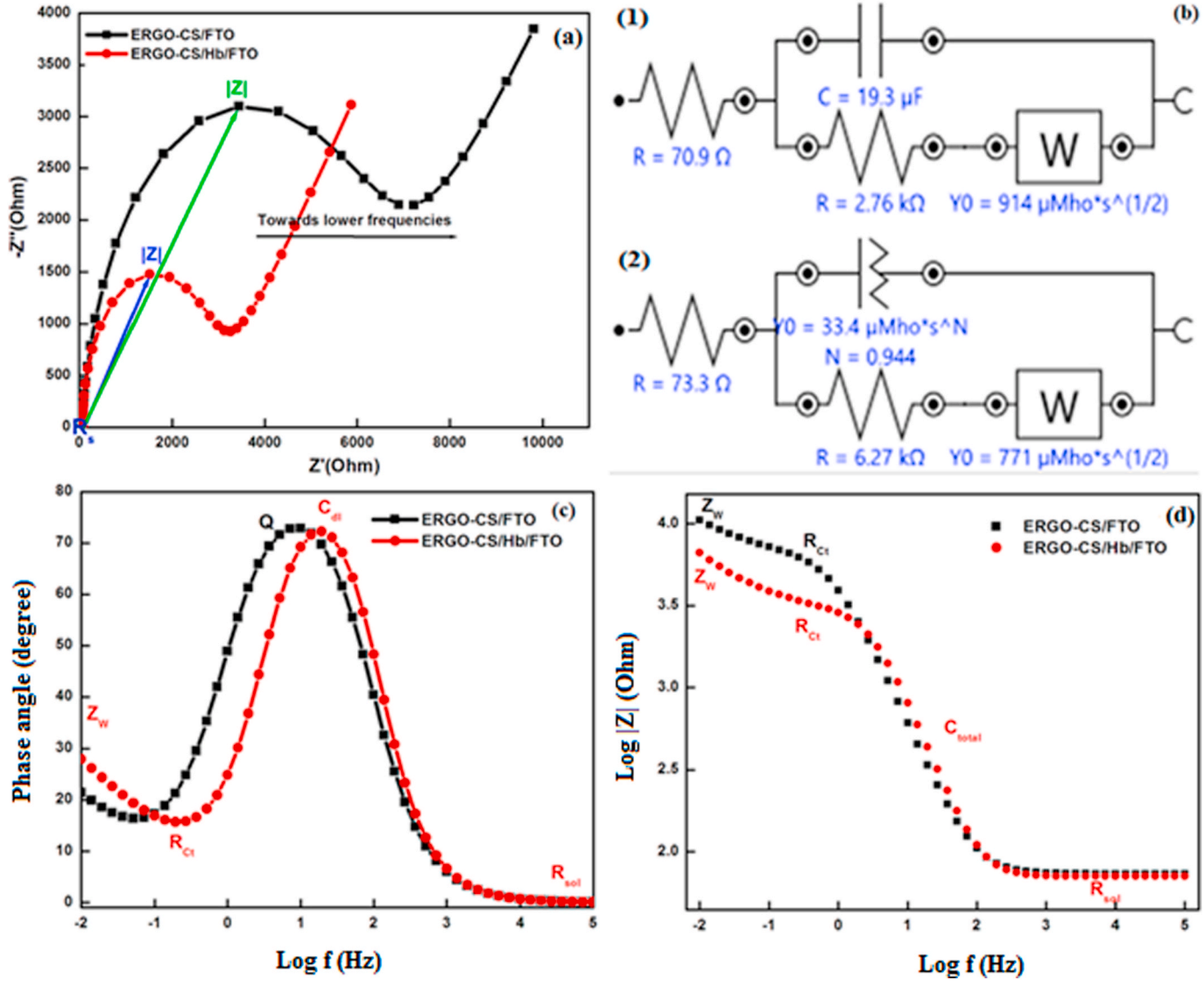

Fig. 4. Electrochemical impedance spectra comprising of (a) nyquist plots, (b) equivalent circuits, and (c,d) bode plots of ERGO-CS/FTO and ERGO-CS/Hb/FTO electrodes.

errors due to capacitive electrochemical double layer. Sometimes solid electrodes that are basically non-ideally polarizable suffer from inhomogeneity and are modelled using constant phase element (CPE) that offers lesser errors and more precise R_{CT} values (Randviir and Banks, 2013; Sun et al., 2015). The R_S and R_{CT} values of ERGO-CS/Hb/FTO are much lower than that of ERGO-CS/FTO attributed to enhanced charge transfer capability enabled by Hb. The different parameters obtained using the randles-equivalent circuit fit are shown in Table S1. It can be seen in phase angle plot (Fig. 4(c)) that a small shift in phase is observed after the immobilization of Hb onto the surface of ERGO-CS/FTO due to altered charge transfer rate as well as change in capacitive behavior. Fig. 4(d) shows that the value of R_{ct} decreases after the immobilization of Hb, contributing towards the enhanced rate transfer.

3.7. Optimization of parameters

The analytical response of biosensor for MP detection was monitored using SWV and Taguchi analysis and in this regard various parameters have been investigated.

3.7.1. Design of experiment and Taguchi optimization

In order to have a closer look at the effect of variation of different parameters in redox response, Taguchi optimization was carried out by selecting a proper design for experimental calculations (Nia et al., 2018). Also, the proposed design and methodology offers the effect of deposition potential, deposition time and pH of the solution towards the redox response of HbFe(I)/HbFe(II). The optimal factor/level combinations of −1.4, 80 and 7 for deposition potential, deposition time and pH values respectively were approved for attaining maximum current response as shown in Fig. S7(See ESM). The analysis predict deposition potential to be most effective parameter whereas pH is the mediator one.

3.7.2. Selection of pH of electrolytic media

The SWV response of ERGO-CS/Hb/FTO was subjected to change in pH of electrolytic media PBS (0.1 M) from pH 5 to pH 9. Both amperometric response as well as peak potential of the fabricated electrodes show the pH-dependent behavior. With increase of pH, the peak potential is shifted towards more negative potentials. Also, the system exhibited two linear ranges with slopes of 13 mV at lower potentials and 72 mV at higher potentials. This break is due to protonation-deprotonation equilibrium related to pK_a of Hb (Urzúa et al., 2018). Further, if we look at the current response, the maximum value is obtained at neutral pH indicating the rupture of Hb morphology in higher basic and acidic media (Fig. S8). So, pH of 7 was utilized for the analytical studies.

3.7.3. Deposition potential and time

For attaining maximum sensitivity, the deposition potential was varied form −0.2 V to −1.6 V followed by SWV response in the potential range of −1.2 V to +0.2 V in the 0.304 μM of MP. It is clearly perceptible that maximum amperometric response was seen at −1.4 V, so this potential was selected for further studies (Fig. S9a). The response of ERGO-CS/Hb/FTO modified electrode was also seen as a function of deposition time. The amperometric response increases with increase in deposition time. To have good agreement between analysis time and sensitivity obtained, 50 s were selected as optimal time for further studies (Fig. S9b).

3.8. Analytical performance of biosensor

The analytical response of ERGO-CS/Hb/FTO was recorded under the optimized conditions (deposition potential of −1.4 V, deposition time 50 s in 1 M PBS (pH 6)) using SWV. SWV response with varying concentrations of MP was monitored using standard addition method. A cathodic response at −0.83 V was observed which is ascribed to the formation of highly reduced form of Hb (HbFe(I)). The enhanced current in these cases thus are attributable to the existence of redox couple of HbFe(I)/HbFe(II) (Jović-Jovičić et al., 2017)[51] (Fig. 5).

On adding MP, the peak current corresponding to the formation of HbFe(I) decreases (Fig. 5(a)) because of the hindered electron transfer between the electrolyte and the electrode surface caused by MP.

The distinct mechanism of electroreduction of HbFe(II) and inhibition of current response on the electrode surface is not very clear. However, the inhibition of Hb in ERGO-CS/Hb/FTO takes place as:

$$\mathrm{HbFe(II)} + e^- \rightarrow \mathrm{HbFe(I)} \quad (3)$$

HbFe(II) binds to O_2 to give HbO_2 in reversible manner as expressed below:

$$\mathrm{HbFe(II)} + O_2 \rightarrow \mathrm{HbFeO_2} \quad (4)$$

In presence of MP which is a nitroaromatic OP, the $HbFeO_2$ gets oxidized to met-Hb shifting the equilibrium in Eq. (4) to right side (Norambuena et al., 1994). This will decrease the amount of HbFe(II) and corresponding electroreduction current is minimized. The formation of met-Hb can also be supported by the fact that the exposure of OPs and nitro compounds to Hb cause methemoglobinemia providing evidence for converting $HbFeO_2$ to met-Hb and thus causing the disease (Sosnowska et al., 2013).

$$\mathrm{HbFeO_2} + \mathrm{MP(R{-}NO_2)} \rightarrow \mathrm{met\text{-}Hb} + \mathrm{R{-}NO_2^-} + O_2 \quad (5)$$

However, in the presence of oxygen,

$$\mathrm{R{-}NO_2^-} + O_2 \rightarrow \mathrm{R{-}NO_2} + O_2^- \quad (6)$$

Following this, the inhibition (%) increases with the increase in concentration of MP from 0.076 μM to 0.988 μM, after which no change in cathodic current was observed on further addition. The calibration plot was generated by plotting a graph between inhibition (%) and concentration of MP. Data fitting of calibration plot gives limit of detection of 79.77 nM, correlation coefficient ($R^2 = 0.99$) and sensitivity of 45.77 $Acm^{-2}\mu M^{-1}$. The limit of detection (calculated using 3σ method) offered here is quite lower in comparison to the values reported in literature (Table 1) that shows its superiority over other biosensors.

3.9. Repeatability, reproducibility, stability and anti-interference ability

In order to appraise the indentation in results, repeatability and reproducibility have been evaluated. The relative standard deviation (RSD) for reproducibility is approximately 2.37% (n = 6) which is acceptable as this might be due to some unavoidable errors during the measurement procedure (Fig. S10(a)). For repeatability, SWVs were recorded for six consecutive measurements showing appreciably stable results with RSD of about 3% (n = 6) (Fig. S10(b)). The biological moieties undergo denaturation or loss of their electrochemical response with increasing span of time. So, the SWV response was checked over a number of days and a fall in current of 4.2% was observed after 7 days, while 93.4% and 92.5% of current was retained even after 14 and 21 days. This indicates the acceptable stability of the prepared sensor (Fig. S10(c)).

To evaluate the usage of developed sensor for food sample analysis, the interference effect of some compounds which show structural intimacy with MP (picric acid, aminophenol, trinitrotoluene, resorcinol and phenol) was also investigated (Fig. S10(d)). It was observed that the presence of these compounds does not offer any interference thus making the fabricated biosensor a selective candidate for food analysis.

3.10. Real sample detection

To check the authenticity of the developed biosensor towards complex samples, the real samples were collected from local market and spiked with the different concentrations of MP. Table S4 shows the recovery % of real samples spiked with different concentrations of analyte

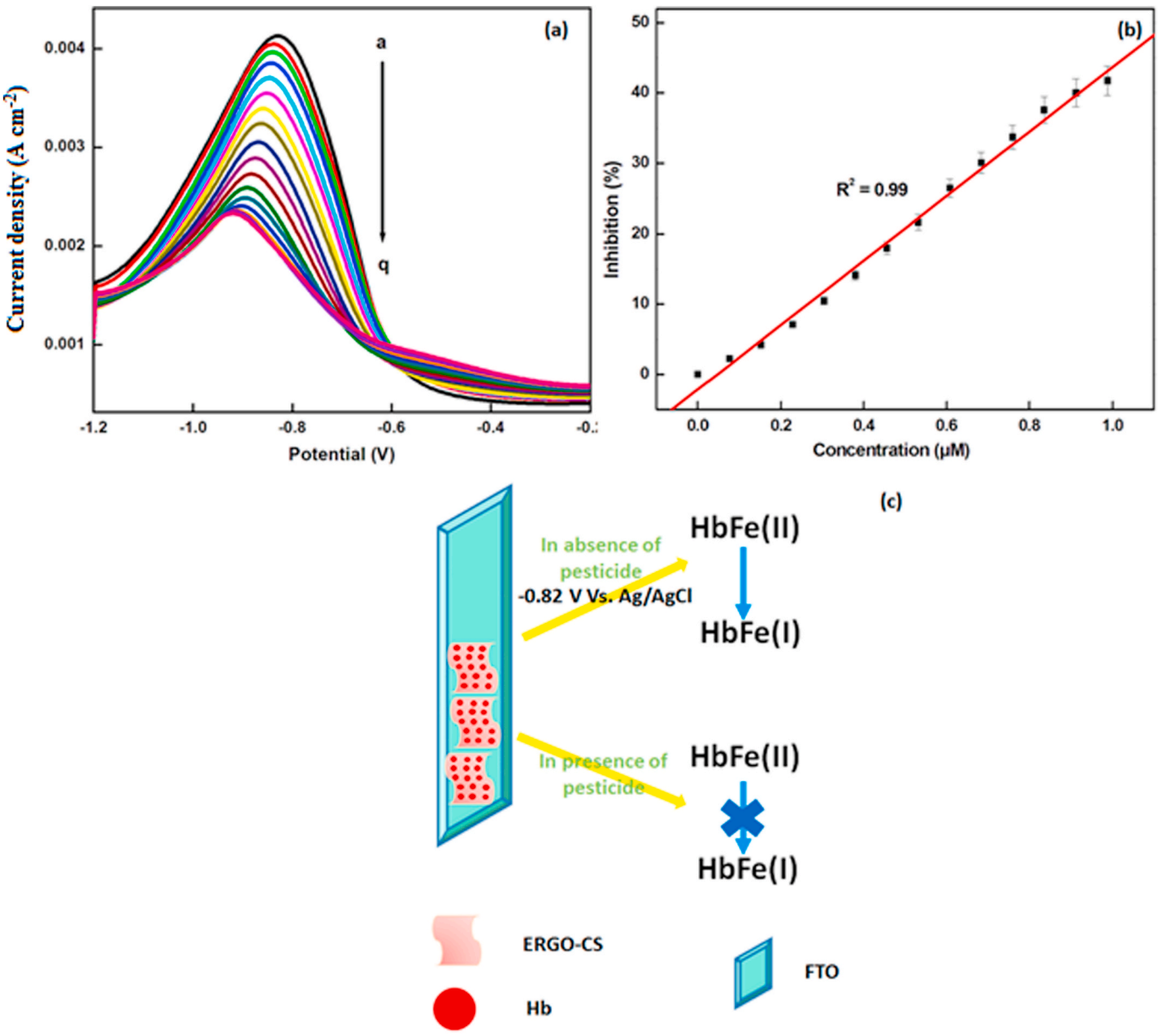

Fig. 5. (a) SWV of ERGO-CS/Hb/FTO in the presence of different concentrations of MP a to q (0–1.216 μM), (b) calibration plot between the linear range of 0.076 μM–0.988 μM and (c) mechanism showing the cause of electrode reactions in the absence and presence of MP.

towards the ERGO-CS/Hb/FTO modified electrode. The average recovery % ranging from 94% to 101%, indicates the good applicability of the prepared biosensor even in complex samples.

4. Conclusion

The redox chemistry involved in the inhibition of HbFe(II)/HbFe(I) process has been successfully utilized for the determination of a nitroaromatic pesticide MP, by designing a novel bioelectrode (ERGO-CS/Hb/FTO) using a green synthetic approach. The synergistic combination offered by both ERGO and Hb on a biocompatible surface has manifested in a faster electron transfer rate in the electrode, ultimately contributing to the excellent performance towards MP sensing. The biosensor thus prepared is equipped with the sensitivity of 45.77 $Acm^{-2}\mu M^{-1}$ that can evaluate MP with limit of detection of 79.77 nM. An adequate reproducibility, repeatability and anti-interfering ability shown by the designed biosensor along with successful application to real time monitoring in vegetable samples has paved its way for practical utility. Hence, biocompatibility and simple synthetic strategy integrated with excellent sensing attributes, involved in the development of ERGO-CS/Hb/FTO electrode can be glorified by utilizing Hb collocation with other nanocomposites for the detection of MP in future projects.

CRediT authorship contribution statement

Ranjeet Kaur: Methodology, Data curation, Writing - original draft. **Shweta Rana:** Conceptualization, Writing - review & editing, Supervision. **Kanika Lalit:** Investigation, Data curation. **Parkash Singh:** Software, Validation. **Khushwinder Kaur:** Visualization, Investigation.

Declaration of competing interest

The authors declare that they have no known competing financial interests or personal relationships that could have appeared to influence the work reported in this paper.

Table 1
Comparison of various electrodes used for the detection of MP based electrochemical sensors.

S. No.	Electrode material	Electrolyte	Linear range (μM)	Limit of detection (nM)	Reference
1	Lipase/CPE	Phosphate buffer	0.038–0.266	100	Reddy et al. (2013)
2	AChE/SnO_2 cMWCNTs/Cu	Phosphate buffer	1–160	100	(Dhull et al., 2018)
3	Pd/MWCNTs	Phosphate buffer	0.37–51.8	189	Huang et al. (2010)
4	AuNP-MWCNTs	Phosphate buffer	(1.89–60.5) $\times 10^3$	189 $\times 10^3$	Ma and Zhang (2011)
5	SA-GCE	B-R buffer	2.07–12.42	950	(Nancy Nirmala et al., 2010)
6	ERGO-CS/Hb/FTO	Phosphate buffer	0.076–0.988	79.77	This work

Acknowledgments:

Ranjeet Kaur acknowledges council of scientific and industrial research (CSIR), New Delhi for providing financial assistance (No. 09/135(0826)/2018-EMR-I dated 06-02-2019). Authors are thankful to Dr. Goutam Sheet, IISER Mohali and Veerpal Kaur, IISER Mohali for AFM measurements.

Appendix A. Supplementary data

Supplementary data to this article can be found online at https://doi.org/10.1016/j.bios.2020.112486.

References

Ahmad, R., Wolfbeis, O.S., Hahn, Y.-B., Alshareef, H.N., Torsi, L., Salama, K.N., 2018. Mater. Today Commun. 17, 289–321.
Aliyev, E., Filiz, V., Khan, M.M., Lee, Y.J., Abetz, C., Abetz, V., 2019. Nanomaterials 9 (8), 1180–1195.
Arjmand, M., Saghafifar, H., Alijanianzadeh, M., Soltanolkotabi, M., 2017. Sens. Actuators B-Chem. 249, 523–532.
Balsebre, A., Baez, M.E., Martinez, J., Fuentes, E., 2018. J. Chromatogr. A 1567, 47–54.
Baranwal, A., Kumar, A., Priyadharshini, A., Oggu, G.S., Bhatnagar, I., Srivastava, A., Chandra, P., 2018. Int. J. Biol. Macromol. 110, 110–123.
Derbalah, A., Chidya, R., Jadoon, W., Sakugawa, H., 2019. J. Environ. Sci. 79, 135–152.
Dhull, V., 2018. Int. J. Anal. Chem. 2874059, 2018.
Facure, M.H.M., Mercante, L.A., Mattoso, L.H.C., Correa, D.S., 2017. Talanta 167, 59–66.
Fotouhi, L., Hashkavayi, A.B., Heravi, M.M., 2012. J. Exp. Nanosci. 8 (7–8), 947–956.
Govindasamy, M., Sakthinathan, S., Chen, S.-M., Chiu, T.-W., Sathiyan, A., Merlin, J.P., 2017. Electroanalysis 29 (8), 1950–1960.
Huang, B., Zhang, W.-D., Chen, C.-H., Yu, Y.-X., 2010. Microchim. Acta 171 (1–2), 57–62.
Hummers, W.S., Offeman, R.E., 1958. J. Am. Chem. Soc. 80, 1339-1339.
Jana, S., Samai, S., Mitra, B.C., Bera, P., Mondal, A., 2014. Dalton Trans. 43 (34), 13096–13104.
Jeyapragasam, T., Saraswathi, R., Chen, S.-M., Lou, B.-S., 2013. Int. J. Electrochem. Sci. 8, 12353–12366.
Jia, M., Liang, F., Jiao, J., Li, S., Hu, J., 2013. J. Solid State Electrochem. 17, 655–660.
Jović-Jovičić, N., Mojović, Z., Mojović, M., Banković, P., Ajduković, M., Milutinović-Nikolić, A., Jovanović, D., 2017. Appl. Surf. Sci. 400, 347–354.
Kovida, Sharma, V., Koner, A.L., 2020. Analyst 4335–4340, 145.
Lavanya, J., Subbiah, A., Neogi, S., Gomathi, N., 2018. Sens. Actuators B-Chem. 255, 536–543.
Lima, A.P., Catto, A.C., Longo, E., Nossol, E., Richter, E.M., Munoz, R.A.A., 2019. Electrochim. Acta 299, 762–771.
Ma, J.-C., Zhang, W.-D., 2011. Microchim. Acta 175 (3–4), 309–314.
Mani, V., Govindasamy, M., Chen, S.M., Chen, T.W., Kumar, A.S., Huang, S.T., 2017. Sci. Rep. 7 (1), 11910.
Navaee, A., Salimi, A., 2015. RSC Adv. 5 (74), 59874–59880.
Nia, P.M., Abouzari-Lotf, E., Arshad, A., Nasef, M.M., Ripin, A., 2018. J. Electrochem. Soc. 165 (9), 429–438.
Nirmala, N.J., Kumaravel, A., Chandrasekaran, M., 2010. J. Appl. Electrochem. 40 (8), 1571–1574.
Norambuena, E., Videla, L.A., Lissi, E.A., 1994. Hum. Exp. Toxicol. 13, 345–351.
Patel, H., Rawtani, D., Agrawal, Y.K., 2019. Trends Food Sci. Technol. 85, 78–91.
Prabhakar, N., Thakur, H., Bharti, A., Kaur, N., 2016. Anal. Chim. Acta 939, 108–116.
Qiao, L., Qian, S., Wang, Y., Lin, H., 2018. Talanta 181, 305–310.
Rana, S., Kaur, R., Jain, R., Prabhakar, N., 2019. Arab. J. Chem. 12 (7), 1121–1133.
Randviir, E.P., Banks, C.E., 2013. Anal. Methods 5 (5), 1098.
Reddy, K.G., Madhavi, G., Swamy, B.E.K., Reddy, S., Reddy, A.V.B., Madhavi, V., 2013. J. Mol. Liq. 180, 26–30.
Rodriguez, S.T., Grosu, I., Crisan, M., Ţifrea, I., 2018. Physica E Low dimens. Syst. Nanostruct. 96, 1–5.
Sahub, C., Tuntulani, T., Nhujak, T., Tomapatanaget, B., 2018. Sens. Actuators B-Chem. 258, 88–97.
Shan, D., Wang, S., Xue, H., Cosnier, S., 2007. Electrochem. Commun. 9 (4), 529–534.
Shanmugharaj, A.M., Yoon, J.H., Yang, W.J., Ryu, S.H., 2013. J. Colloid Interface Sci. 401, 148–154.
Sosnowska, B., Huras, B., Nowacka-Krukowska, H., Bukowska, B., 2013. Biologia 68, 773–778.
Sun, C., Wang, D., Zhang, M., Ni, Y., Shen, X., Song, Y., Geng, Z., Xu, W., Liu, F., Mao, C., 2015. Analyst 140 (3), 797–802.
Thomas, D., Rasheed, Z., Jagan, J.S., Kumar, K.G., 2015. J. Food Sci. Technol. 52 (10), 6719–6726.
Thota, R., Ganesh, V., 2016. Sens. Actuators B-Chem. Chemical 227, 169–177.
Tian, X., Liu, L., Li, Y., Yang, C., Zhou, Z., Nie, Y., Wang, Y., 2018. Sens. Actuators B-Chem. 256, 135–142.
Toh, S.Y., Loh, K.S., Kamarudin, S.K., Daud, W.R.W., 2014. Chem. Eng. 251, 422–434.
Urzúa, L., Pérez-Ortiz, M., Álvarez-Lueje, A., 2018. J. Chil. 63, 3914–3917.
Wang, L., Zhang, Y., Wu, A., Wei, G., 2017. Anal. Chim. Acta 985, 24–40.
Wen, Y., Wen, W., Zhang, X., Wang, S., 2016. Biosens. Bioelectron. 79, 894–900.
WHO, 2009. International Programme on Chemical Safety. Geneva.
Xu, Z.-L., Deng, H., Deng, X.-F., Yang, J.-Y., Jiang, Y.-M., Zeng, D.-P., Huang, F., Shen, Y.-D., Lei, H.-T., Wang, H., Sun, Y.-M., 2012. Food Chem. 131 (4), 1569–1576.
Zangmeister, R.A., Park, J.J., Rubloff, G.W., Tarlov, M.J., 2006. Electrochim. Acta 51 (25), 5324–5333.
Zhang, H.-P., Luo, X.-G., Lin, X.-Y., Lu, X., Tang, Y., 2016. Appl. Surf. Sci. 360, 715–721.
Zhang, L., Han, G., Liu, Y., Tang, J., Tang, W., 2014. Sens. Actuators B-Chem. 197, 164–171.